Multi-mode ground state cooling of trapped ions

Von der QUEST-Leibniz-Forschungsschule
der Gottfried Wilhelm Leibniz Universität
Hannover

zur Erlangung des Grades
Doktor der Naturwissenschaften
Dr. rer. nat.

genehmigte Dissertation
von

Nils Scharnhorst, M.Sc.
geboren am 06.12.1986 in Hannover

2018

Kurzfassung

Innerhalb dieser kumulativen Dissertation präsentiere ich die Ergebnisse meiner Doktorarbeit in Form von drei Publikationen. Im Zusammenhang eines ^{27}Al$^+$/^{40}Ca$^+$ Quantenlogik Uhrenexperiments wurde ein Transferstabilisierungsschema entwickelt und demonstriert. Dieses ermöglicht die Phasenstabilität eines ultrastabilen Masterlasers mit hoher Bandbreite auf Laser unterschiedlicher Wellenlänge mittels eines Frequenzkamms zu übertragen. Die hohe Bandbreite wird ohne Vorstabilisierung der Laser auf Resonatoren bei ihrer jeweiligen Wellenlänge erreicht, indem das intrinsische Phasenrauschen des Frequenzkamms elektronisch subtrahiert wird. Die erfolgreiche Umsetzung des Transferstabilisierungsschemas wird anhand von Phasenrauschmessungen mittels eines Resonators und von Rabi Oszillationen auf dem Logikübergang von ^{40}Ca$^+$ demonstriert, welche von einem auf einen Masterlaser bei 1542 nm stabilisierten Lasers bei 729 nm getrieben werden.

Durch das Transferstabilisierungsschema sind alle Laser, welche auf denselben Masterlaser phasenstabilisert sind, auch untereinander phasenstabil. Dies ermöglichte die Umsetzung eines neuartigen Kühlschematas namens "double bright electromagnetically induced transparency (EIT) Kühlen" (D-EIT). Es wurde im Rahmen dieser Arbeit entwickelt und erweitert das konventionelle EIT Kühlenschema zu einer M-förmigen Niveaustruktur mit drei Grund- und zwei angeregten Zuständen. Im "dressed states"-Bild enthält D-EIT einen Dunkelzustand zur Unterdrückung von Trägerstreuung und zwei individuell verschiebbare Hellzustände. Im Falle eines gefangenen ^{40}Ca$^+$ Ions werden die Hellzustände in Resonanz mit den axialen und radialen Moden gebracht, welche mehr als 1,6 MHz auseinander liegen. Hierdurch konnte Grundzustandskühlen aller drei Bewegungsfreiheitsgrade innerhalb eines einzelnen Kühlpulses demonstriert werden. Das M-Niveau Schema von D-EIT wird durch Laser bei 866 nm und 397 nm gebildet, zwischen denen eine feste Phasenbeziehung bestehen muss, um den Dunkelzustand erzeugen zu können. Erfolgreiches D-EIT Kühlen stellt demnach einen indirekten Nachweis für das Funktionieren des Transferstabilisierungsschematas für Laser dar, deren Frequenzen mehr als eine Oktave auseinander liegen. Die erreichbaren Kühlraten und die mittleren Gleichgewichts-Bewegungsquantenzahlen nach dem D-EIT Kühlen werden mit denen von Standard EIT verglichen und deren jeweiligen Limitierungen diskutiert.

Abschließend werden die gewonnenen Erkenntnisse verwendet, um die Uhrenperformance einer ^{27}Al$^+$ Quantenlogikuhr in Bezug auf die Schwarzkörperverschiebung, die Zeitdilatationsverschiebung, die ac-Stark Verschiebung durch die Kühllaser und der Verschiebung durch Exzessmikrobewegung abzuschätzen.

Schlagwörter: Uhren, Laserstabilisierung, Transferstabilisierung, Grundzustandskühlen, Multimodenkühlen, EIT Kühlen, Doppel EIT Kühlen

Abstract

Within this cumulative thesis I present the results of my work as a PhD student in the form of three publications. In the context of an $^{27}\text{Al}^+/^{40}\text{Ca}^+$ ion optical clock experiment a transfer-locking scheme has been developed and demonstrated. It allows the transfer of phase stability from an ultra-stable master laser to lasers of different wavelengths via a frequency comb. The intrinsic noise of the frequency comb is electronically subtracted, allowing high-bandwidth transfer of the phase stability from the master to the slave lasers and removing the need for auxiliary reference cavities for laser pre-stabilization at each slave laser's wavelength. The successful implementation of the transfer-locking scheme is demonstrated by phase-noise measurements on an external cavity of a 729 nm slave laser locked to a master laser at 1542 nm, and by measurements of Rabi flops on the logic transition in a single $^{40}\text{Ca}^+$ ion, driven by the 729 nm slave laser.

As a consequence of the transfer-locking scheme, all lasers that are phase-locked to the master laser are also phase-stable with respect to each other. This allowed the implementation of a novel cooling scheme termed double bright electromagnetically induced transparency (EIT) cooling (D-EIT). It extends conventional EIT cooling to an M-shaped level-structure with three ground states and two excited states, which has been developed within this thesis. In the dressed state picture, D-EIT cooling provides one dark state to suppress carrier scattering and two individually shiftable bright states. For the case of a trapped single $^{40}\text{Ca}^+$ ion, the two bright states have been shifted into resonance with the axial and radial modes, being more than 1.6 MHz apart. That way ground state cooling of all three motional degrees of freedom within a single cooling pulse has been demonstrated. The M-level system of D-EIT cooling is formed by beams at 866 nm and 397 nm and requires a stable phase relation between them in order to create the dark state. This indirectly confirms the functioning of the transfer-locking scheme for lasers with frequencies separated by more than one octave. The achievable cooling rates and steady-state mean motional quantum numbers after D-EIT cooling are compared to those of standard single EIT cooling. The limitations of each cooling scheme are investigated.

Finally, the results are employed to estimate the clock performance of an $^{27}\text{Al}^+$ quantum logic clock with respect to the black-body radiation shift, the time-dilation shift, the ac-Stark shift due to cooling lasers, and excess micromotion.

Key words: Clocks, Laser Stabilization, Transfer-Lock, Ground State Cooling, Multi-mode Ground State Cooling, EIT cooling, Double-Bright EIT cooling

Declaration

I hereby declare that this thesis is my own work and effort and that it has not been submitted anywhere for any award. Where other sources of information have been used, they have been acknowledged.

Braunschweig, 30.11.2017   Nils Scharnhorst

Contents

Acronyms

AC	alternating current
AOM	acousto optical modulator
BBR	black-body radiation
BSB	blue sideband
CGPM	General Conference of Weights and Measures
CW	continuous wave
DC	direct current
D-EIT	double-bright EIT cooling
DDS	direct digital synthesizer
ECDL	external cavity diode laser
EDFA	erbium doped fiber amplifier
EIT	electromagnetically induced transparency
EMM	excess micromotion
EOM	electro optical modulator
FPGA	field programmable gate array
FWHM	full width half maximum
GSC	ground state cooling
OOP	out-of-phase
PCF	photonic crystal fiber
PD	photo detector
PID	proportional-integral-derivative
PLL	phase locked loop
PMT	photomultiplier tube
PSD	phase noise spectral density
PTB	Physikalisch-Technische Bundesanstalt
QUEST	Centre for Quantum Engineering and Space-Time Research
RF	radio frequency
RSB	red sideband
SI	International System of Units
UV	ultraviolet

1 Introduction

Time is ubiquitous in everyday life. Although intangible, it is essential for the definition of other metric units. Today, even the unit of length is defined via the time light needs to travel a specific distance [1]. With the upcoming redefinition of the international system of units (SI) the second will become part of the definition of all SI units except the Mol [2]. Therefore, it is particularly important to make the measurement of time as practical and as precise as possible. Arthur Schawlow famously put it: "Never measure anything but frequency" [3]. By this he meant that frequency measurements can be performed with the highest precision of all measurable quantities. Therefore, whenever possible, experiments should be designed to measure the desired quantity as a frequency to obtain the lowest possible uncertainty on that quantity. Since time is the inverse of frequency it becomes immediately clear that time should be determined by a frequency. Then, the second can be defined as the time a specific oscillator needs to undergo a certain number of oscillations.

An oscillator is called a *frequency standard* if its frequency is stable and can be traced back to the definition of the second. If a frequency standard can additionally display its measured time, it is called a *clock*. Clocks continuously count the number of evolved cycles from a well-defined starting time. To understand this definition, the term "stable oscillator" has to be specified further. In order to quantify the performance of an oscillator, its frequency has to be compared to a reference which, for the sake of argument, is assumed to have a constant and known frequency. An oscillator is called the more *stable* the smaller the variations of its frequency around its average value are. The difference between the expected and the measured frequency is called *accuracy*.

The SI second itself should be determined by the best performing clock. Ideally, the oscillator of the clock has a constant frequency and that frequency is counted with minimal error. From the medieval era up to 1967, time was related to astronomical events and the last astronomical definition of the second read "the fraction 1/31,556,925.9747 of the tropical year for 1900 January 0 at 12 hours ephemeris time" using the periodicity of the earth's orbit around the sun as oscillator. In terms of practicability, this definition is inconvenient since it cannot be reproduced and the precision of this astronomical clock is questionable due to the changing earth's orbital period. Therefore, in 1967 the SI second was redefined to be "the duration of 9,192,631,770 periods of the radiation

corresponding to the transition between the two hyperfine levels of the ground state of the cesium-133 atom" which is still the valid definition of the second at the time of this thesis. The common way to realize the second according to that definition is to use a microwave-oscillator whose frequency is regularly compared to the reference transition in ^{133}Cs in spectroscopy experiments. The difference between the oscillator's frequency and the reference transition frequency is used as a feedback signal for the stabilization of the oscillator's frequency to that reference transition frequency.

The maximum achievable stability of an atomic clock is limited by the linewidth of the reference transition and its absolute frequency. Given similar linewidths, optical reference transitions – accessible by lasers instead of microwave oscillators – have 10^4 to 10^5 times more cycles per second compared to microwave atomic transitions and thus potentially provide better stability. With the invention of the frequency comb [3], it became possible to downscale optical frequencies to the radio frequency range, where they can be further processed and counted electronically, allowing the construction of optical clocks. Apart from using an optical instead of a microwave transition, the working principle of optical clocks is the same as that of microwave clocks. Nowadays, optical clocks have surpassed microwave clocks in terms of stability and accuracy by more than one order of magnitude, see e.g. [4–6].

Optical frequency standards and clocks can be used for tests of new physics such as the variation of fundamental constants in time [7–12], studies of many-body quantum systems [13, 14], and the search for cosmic domain wall dark matter [15]. Clocks play an important role in global navigation satellite systems (GNSS) [16, 17], and relativistic geodesy [18–20]. All these applications benefit from more stable and more accurate clocks.

As a consequence of the development of optical frequency standards, a redefinition of the SI second is currently under discussion [2, 4]. Different atomic species and clock types are being considered to replace the cesium clock as the primary standard for the second. Amongst these candidates are clocks based on a transition in aluminum ions (^{27}Al$^+$). Ions in general have the advantage that they can be trapped and stored via electromagnetic fields, which do not couple to the ion's internal degrees of freedom. This allows to isolate trapped ions from the environment, and thus rendering them a highly accurate reference for the oscillator of the clock. Aluminum in particular is a promising clock ion since its clock transition at 267 nm has a high absolute frequency and is narrow ($2\pi \times 8$ mHz), thus providing a high quality factor. Additionally, the ^{27}Al$^+$ clock transition has the smallest known blackbody shift amongst all considered elements, and a negligible quadrupole shift [21]. Unfortunately, the transition that would normally be used for Doppler cooling and state read-out is at 167 nm, which is in the deep ultra-violet (UV) and inaccessible to currently available lasers. As a solution, aluminum

is stored together with a second, so-called spectroscopy or logic ion, which possesses an amenable cooling transition and whose states can be used for state discrimination. If both ions are stored together in the same trapping potential, cooling of the logic ion sympathetically cools the aluminum ion via the Coulomb interaction. Via quantum logic spectroscopy [22], the internal state of the aluminum clock ion can be transferred to the logic ion using their shared vibrational modes. Different species fulfill the requirements for a logic ion and in our setup calcium ($^{40}Ca^+$) has been chosen [23].

In order to convert the clock laser frequency down to a countable radio frequency, the experimental clock setup includes a frequency comb with outputs at the wavelengths of all lasers required for spectroscopy of calcium and aluminum ions. A frequency comb itself is a pulsed laser that can be stabilized to an ultra-stable optical reference (master). Within this thesis, a transfer-locking schemes has been developed [24], see Sec. 2.1, to phase-stabilize the other continuous wave (CW) lasers in the experiment to the same master. The frequency comb serves as a gear box to bridge the frequency difference between master and slave lasers, while intrinsic noise of the frequency comb is removed up to high bandwidths. For this, the lasers themselves do not need to be pre-stabilized by external cavities. Since all transfer-locked lasers are phase stable to the same master, they are also phase stable with respect to each other, even though the wavelength differences among them exceeds one octave. Relative phase stability over such large wavelength differences cannot be achieve by previous techniques such as e.g. transfer cavities [25, 26] due to the limited spectral bandwidth of one cavity mirror set.

Perturbations of the clock transition induced by external fields and motion have to be either suppressed or evaluated and corrected in order to achieve the desired accuracy and stability of the frequency standard. Due to the weak coupling of the $^{27}Al^+$ clock transition to the environment [21], motion-induced shifts dominate the error budget for an $^{27}Al^+$ clock [27]. Motion of the ion leads to a second order Doppler shift – also known as time-dilation shift – of the clock transition frequency as a result of the mismatch between the moving ion's proper time and the lab-frame time. Thus, uncertainty in the motion decreases the clock's accuracy and imposes a limitation of the fidelity of the quantum logic spectroscopy scheme. Therefore, it is preferable to cool the ions' motion close to the motional ground state – ideally for all six motional degrees of the two ion crystal.

Thanks to the transfer-locking scheme, it became possible to develop double-bright electromagnetically induced transparency (D-EIT) cooling [28, 29] within this thesis as a novel scalable variation of standard electromagnetically induced transparency (EIT) cooling. D-EIT extends the usual EIT Λ level scheme by one additional ground and one excited state. D-EIT allows simultaneous ground state cooling (GSC) of modes around two separated frequencies. In this thesis, this capability is used for the first experimental

demonstration of GSC of all three motional degrees of freedom of a trapped ion within a single cooling pulse. For D-EIT cooling, three ground states and two excited states are coherently connected in a double-Λ level scheme by lasers at $397\,\mathrm{nm}$ and $866\,\mathrm{nm}$, a scheme made possible by the transfer-locking technique described above. The D-EIT scheme enables cooling of spectrally separated modes and may allow simultaneous GSC of all six modes of the $^{27}\mathrm{Al}^+/^{40}\mathrm{Ca}^+$ ion crystal.

Two established techniques for ground state cooling of ions are sideband cooling (SBC) and EIT cooling. The first of these can only cool one mode at a time while the latter is capable of cooling modes within a narrow frequency range. Cooling of several modes within one EIT pulse has been demonstrated experimentally [30]. EIT cooling is fast compared to sideband cooling since carrier scattering is suppressed by a dark resonance. For both cooling schemes, the cooling rate scales with the intensity of the cooling lasers. However, increasing intensities lead to power-broadening of the cooling resonance, which results in increased off-resonant carrier-scattering. Carrier transitions do not contribute to cooling and if the system is close to its motional ground state carrier transitions lead to heating since a decay on the blue motional sideband becomes more likely than on the red motional sideband. This reduces the cooling rate and limits the achievable minimum temperature of the system. As a consequence, in sideband cooling the intensities of the cooling lasers has to be limited to curb the effect of off-resonant carrier scattering. By notching out the scattering spectrum at the carrier, EIT cooling can tolerate power-broadening of the cooling resonance and thereby allows higher cooling rates compared to sideband cooling. Therefore, the work within this thesis focuses on EIT-like cooling and provides an in-depth analysis and comparison between single EIT and double-bright EIT cooling, see Sec. 2.2. The detrimental effect of excited spectator modes in standard EIT cooling is investigated. This effect is avoided in the D-EIT cooling scheme due to the simultaneous cooling of all motional modes of a single $^{40}\mathrm{Ca}^+$ ion. Furthermore, D-EIT cooling overcomes the limitation of off-resonant excitation from superfluous P states in standard EIT cooling by incorporating all relevant electronic excited states in the cooling level scheme. In comparison to standard EIT cooling, this will enable higher cooling rates for systems that operate deep in the Lamb-Dicke regime. The GSC performance, both in cooling rate and steady-state temperature, for D-EIT cooling is investigated and compared with standard EIT cooling. By enabling fast ground state cooling of all six modes of the $^{27}\mathrm{Al}^+/^{40}\mathrm{Ca}^+$ ion crystal, the D-EIT cooling scheme will allow a reduction of motion-induced shifts of the $^{27}\mathrm{Al}^+$ clock, while limiting the experimental dead-time due to cooling to a minimum.

The experimental results of this work can be used to predict parts of the error budget of the $^{27}\mathrm{Al}^+/^{40}\mathrm{Ca}^+$ quantum logic clock. Amongst the largest contributions for clock uncertainties are the black-body radiation shift, the second order Doppler shift due to micromotion and secular motion, and the ac Stark shift caused by lasers cooling the ions during the clock interrogation. In Sec. 2.3, the magnitudes of these shifts are estimated and discussed.

2 Results

This chapter presents the results of this work. Sections 2.1 and 2.2 present the results of the transfer-locking scheme [24] and double-bright EIT cooling [28, 29], respectively, and put them into broader scientific context. These three publications form this cumulative thesis, the author contributions are listed at the end of each of the two section. Finally, Sec. 2.3 presents estimates for systematic effects and their uncertainties for a $^{27}\text{Al}^+/^{40}\text{Ca}^+$ quantum logic clock, based on the measurements obtained during this work.

2.1 High-bandwidth transfer of phase stability through a fiber frequency comb

Optics Express Vol. 23, Issue 15, pp. 19771-19776 (2015)

A frequency comb is an integral part of every optical clock experiment, used to measure absolute (optical) frequencies and convert them into the easier-to-process microwave regime [31]. Consequently, the setup of the ^{27}Al$^+$/^{40}Ca$^+$ quantum logic clock experiment, with which the experiments of this thesis have been conducted, includes a frequency comb with optical outputs covering the spectral range of all lasers necessary to operate the clock. The repetition rate of our frequency comb itself is locked to the same master laser used for the transfer-locking scheme and the offset beat is stabilized to a radio frequency (RF) reference, which is derived from the primary frequency standards at Physikalisch-Technische Bundesanstalt (PTB). Hence, the regularly-spaced teeth of a frequency comb serve as reference to which to stabilize a laser. Figure 2.1 compares the phase noise spectral density (PSD) – after removal of the carrier-envelope-offset noise – of a comb tooth at 729 nm (a) to the PSD of a free-running external-cavity diode laser[a] (ECDL) (b). The PSD of the comb tooth exceeds that of the free-running ECDL for frequencies above 20 kHz, so that locking the ECDL to the comb tooth (c) cannot suppress laser noise past a Fourier frequency of 20 kHz. Hence, the comb's high-frequency noise limits the bandwidth in which it can serve as a useful reference, so that phase-locking of the ECDL to the comb tooth generally requires pre-stabilization to a separate reference cavity

The high-bandwidth transfer-oscillator feed-forward scheme developed in this thesis suppresses the effect of comb noise in an unprecedented 1.8 MHz bandwidth. The suppression is achieved by synthesizing a virtual beat signal between a 1542 nm ultra-stable master laser and the 729 nm diode laser (slave), in which the effect of the comb noise is suppressed by microwave feed-forward electronics. This is a high-bandwidth implementation of the so-called transfer-oscillator lock [32], which circumvents the necessity for a tight comb lock. The result of the phase-lock of the slave via the virtual beat with the master laser is shown in Figure 2.1(d). The transfer-locking scheme suppresses the phase-noise of the ECDL below the free-running level for frequencies up to 200 kHz. Compared to the direct lock to the comb (Figure 2.1(c)), the virtual beat improves the useful locking bandwidth by an order of magnitude.

The practical impact of the transfer-locking scheme is illustrated by carrying out coherent manipulations of a trapped calcium ion with 99 % fidelity even at few-microsecond

---

[a]In the setup, DLpro lasers from Toptica are used, with a specified line-width of around 60-100 kHz.
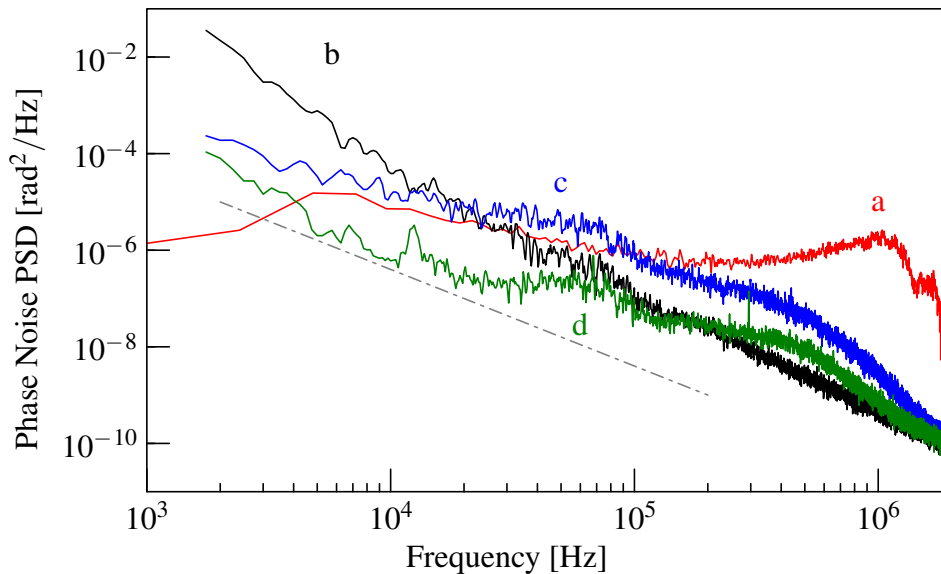
Figure 2.1: Phase noise power spectral density of (a) a comb tooth at 729 nm (after removal of carrier envelope noise) (b) the free-running ECDL, for reference (c) the ECDL locked directly to the 729 nm comb tooth (d) the ECDL locked to the virtual beat with the 1542 nm master laser. The dashed line indicates the measurement noise floor for curves (b-d) due to laser intensity noise. Note the additional noise suppression bandwidth of spectrum (d) compared to that of spectrum (c).

timescales. This shows that the transfer-oscillator locking can provide sufficient phase stability for high-fidelity quantum logic manipulation even without pre-stabilization of the slave diode laser. By eliminating the need for auxiliary reference cavities for laser pre-stabilization at each wavelength, this capability allows a substantial simplification of experimental setups requiring multiple stable lasers, such as high-accuracy frequency standards based on quantum logic spectroscopy [10], experiments in Rydberg spectroscopy [33], or coherent photo-association and control of molecules with Raman pulses [34]. The option to use a single transportable reference cavity [35, 36] for all lasers in a setup potentially will also reduce bulk and weight in proposed portable or space-based optical clocks [37] for tests of fundamental physics [10–12] or relativistic geodesy [18–20].

A beat between the transfer-locked 729 nm laser and an independently cavity-locked 729 nm laser [38] revealed a beat line-width of <160 Hz, while the master laser is expected to have an effective line-width of around 1-10 Hz[b]. The slave laser linewidth is thus not limited by the master laser, but rather by residual comb noise beyond the suppression bandwidth of the transfer-lock feed-forward scheme. The comb noise suppression bandwidth is limited by relative time delays between the different signal paths

---

[b]Gesine Grosche, private communication. Limited by uncanceled fiber noise in the optical path.

that are subtracted from each other in the transfer-locking scheme, while the overall loop delay limits the feedback bandwidth for the laser lock. Here, the overall loop delay is caused by electronic filters in the feedback electronics, necessary to remove or suppress unwanted signals from the error signal. As well as extending the bandwidth of the feed-forward noise subtraction, one might also improve the system's performance by lowering the overall level of comb noise so that there was less of it to subtract in the first place. Intrinsic comb noise is caused by electronic noise as well as external noise, coupling to the free-space optics part of the frequency comb's oscillator. It can be reduced by a tighter comb lock or by protecting the oscillator from environmental perturbations. The former is limited by electronic resonances at around $900\,\mathrm{kHz}$ in the intra-cavity electro-optical modulator used for fast locking feedback, while the latter can for example be achieved by a fully fiberized optical comb, i.e. without any free-space optics.

In general, the comb noise suppression bandwidth imposes a limit on the ability to reduce the PSD of a slave laser with the transfer-locking scheme. For noisier lasers than reported here, the achievable locking bandwidth is reduced and laser stabilization to a cavity [39–41] might outweigh the advantages of the transfer-locking scheme. It is to be noted that, whatever the choice of reference, the stabilization feedback typically imprints servo-bumps onto the spectrum of the stabilized laser.[c] This is true for both, the transfer-locking scheme, as well as for the stabilization to a cavity. These servo-bumps may cause unintentional off-resonant excitation of electronic or vibrational levels, which is especially critical for the interrogation of the logic transitions in aluminium and calcium. These stabilization artifacts could be removed by injection locking a slave laser to the stabilized laser [42] and using the output of the slave laser for the interrogation of the logic transitions.

At the time of writing, the transfer-locking scheme is implemented to phase-lock four different lasers ($729\,\mathrm{nm}$ $^{40}\mathrm{Ca}^+$ logic laser, $267\,\mathrm{nm}$ $^{27}\mathrm{Al}^+$ logic laser, $866\,\mathrm{nm}$ $^{40}\mathrm{Ca}^+$ repumper, and $397\,\mathrm{nm}$ $^{40}\mathrm{Ca}^+$ cooling and detection laser), as well as the repetition rate of the frequency comb itself, to the ultra-stable master laser at $1542\,\mathrm{nm}$. Being phase-locked to the same master laser, all lasers are also phase-stable with respect to each other, independent of the frequency gap between them. This is an advantage over the use of cavities for phase-stability transfer between lasers of different wavelengths [25, 26]. There, the maximum possible spectral gap between the lasers is limited by the spectral bandwidth of the cavity's mirror coatings for optical wavelengths, which usually covers less than an octave. High-contrast dark resonances between the $866\,\mathrm{nm}$ $^{40}\mathrm{Ca}^+$ repumper and the $397\,\mathrm{nm}$ $^{40}\mathrm{Ca}^+$ cooling and detection laser demonstrate high-bandwidth mutual phase-stability between the lasers, being spectrally separated by more than one octave [29]. This facilitates the implementation of D-EIT cooling (see Section 2.2).

---

[c]In our setup, servo-bumps are found roughly $500\,\mathrm{kHz}$ around the carrier.

Contributions

Table 2.1: Author contributions.

Name	Research question/plan	Conducting experiments	Evaluation of results	Preparation of the manuscript
Nils Scharnhorst[1]	✓	✓	✓	✓
Jannes B. Wübbena[1]	✓	✓	✓	✓
Stephan Hannig		✓		✓
Kornelius Jakobsen				✓
Johannes Kramer				✓
Ian D. Leroux	✓	✓	✓	✓
Piet O. Schmidt	✓		✓	✓

[1] Equal contributions.

2.2 Multi-mode double-bright EIT cooling

Multi-mode double-bright EIT cooling, arXiv:1711.00738 (2017)
Experimental and theoretical comparison of the cooling performance between standard and double-bright EIT cooling, arXiv:1711.00732 (2017)

Ground-state cooling (GSC) of ions and atoms is an essential prerequisite for many experiments in quantum optics, optical spectroscopy and clocks, quantum simulations, and quantum information processing. Sideband cooling (SBC) [43–48] and cooling via electromagnetically induced transparency (EIT) [30, 49–52] are the most common techniques to achieve ground state cooling. Cooling performance is characterized by the cooling rate, the minimal achievable kinetic energy, and how many motional modes are cooled simultaneously.

SBC works in the resolved sideband regime, where carrier and motional resonances are spectrally separated. Here, cooling of a particular mode is achieved by tuning a laser into resonance with the corresponding red sideband (RSB). This way, a mode far above its ground state most likely scatters a photon on the RSB, which removes a quantum of motion from the respective mode such that cooling takes place. However, RSB scattering events become less probable the closer the mode gets to its ground state and carrier scattering becomes the dominant scattering event. Carrier scattering does not reduce the motional energy and thus does not contribute to cooling. Moreover, in this regime, carrier scattering effectively limits the minimum steady-state temperature, since the most likely decay channels after a carrier excitation are the carrier itself, and the blue sideband (BSB). BSB scattering adds a quantum of motion to the system and heats the mode up, which limits the possible minimum steady-state temperature of the system.

EIT cooling improves upon the limitations of SBC by suppressing carrier scattering. This is achieved by tuning two mutually phase-stable lasers from two ground states into resonance on one virtual excited state, which is blue detuned with respect to an electronic excited state. The new eigenstates of the combined system are described in the dressed-state picture. In the described Λ-configuration, carrier scattering is suppressed by a dark state. In addition, a bright state is created, which can be shifted into resonance with a motional RSB via the Stark-shifts of the two cooling lasers. Effectively, EIT cooling can be thought of as SBC but without the disadvantages of carrier scattering and therefore leads to higher cooling rates for a given steady-state temperature close to the motional ground state, as illustrated in Figure 2.2, which compares the mean motional quantum number during SBC and single EIT cooling. However, it is not possible to implement EIT cooling in arbitrary systems, because off-resonant coupling to or decay into electronic
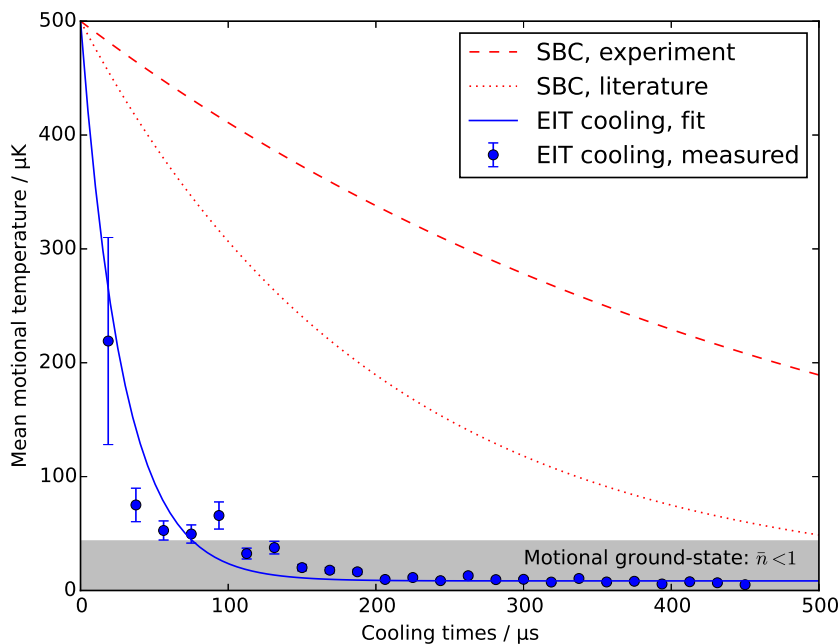
Figure 2.2: Cooling performance comparison of the axial mode of a single ^{40}Ca$^+$ ion between standard EIT (measured, blue data points and line) and sideband cooling (red dashed and dotted lines). The lines are generated via the following model: $T(t) = T_{\text{offset}} + (T_{\text{Doppler}} - T_{\text{offset}}) \exp(-t/\tau)$, where a Doppler temperature $T_{\text{Doppler}} = 500\,\mu$K was assumed, $T_{\text{offset}} = 8.4(8)\,\mu$K was fitted to the data, and τ is the exponential decay constant. The red dashed line represents the fastest SBC realized in the setup with $\tau \approx 500\,\mu$s (taken from [53]), the dashed dotted red line represents the fastest SBC to the motional ground state ($\tau \approx 200\,\mu$s) reported in the literature for a ^{40}Ca$^+$ ion [54]. For EIT cooling $\tau = 28.8(2.8)\,\mu$s is obtained from the fit of the measured data with the above mentioned model.

states outside the Λ-configuration might lead to a decay of the dark state. Another requirement for the successful implementation of EIT cooling are cooling lasers that are phase-stable with respect to each other. Decoherence between the cooling lasers also limits the lifetime of the dark state, thus allowing carrier scattering.

Due to their narrow cooling resonance, both sideband and EIT cooling restrict cooling to a narrow frequency range. However, to scale up the number of ions in quantum systems and to control all relevant (motional) degrees of freedom in such large atomic ensembles demands for novel cooling approaches, such as the capability to cool several motional modes simultaneously.

Within this work, double-bright EIT (D-EIT) cooling has been developed as an extension of standard EIT cooling by adding one additional ground and one excited state to

Table 2.2: Comparison of experimental values for single EIT, concatenated single EIT cooling pulses (3D single EIT, the pulse ordering is given in parenthesis), and D-EIT cooling, each starting from Doppler cooling temperatures and optimized for minimum $\bar{n}$ at $\Delta = 71.5\,\text{MHz}$.

EIT Method	$n_{\text{ss,a}}$	$n_{\text{ss,r}}$	$t_{\text{ss}}\ (\mu\text{s})$
Single EIT ax.	0.10	≈ 7	720
3D Single EIT (first radial, second axial EIT pulse)	0.04	0.20	640[a]
Single EIT rad.	≈ 1.3	0.10	490
3D Single EIT (first axial, second radial EIT pulse)	≈ 1	0.10	700
D-EIT	0.11	0.14	670

[a] Smaller than the sum of t_{ss}, since the axial mode is pre-cooled by the radial pre-cooling pulse.

the cooling level scheme. It allows simultaneous GSC of modes around two separated frequencies. In this thesis this capability is used for the first experimental demonstration of ground state cooling of all three motional degrees of freedom of a trapped ion within a single cooling pulse.

In the publications presented in this section, details on the experimental apparatus are provided, and more importantly, an in-depth analysis and comparison between single EIT and double-bright EIT cooling is given. The detrimental effect of hot spectator modes in standard EIT cooling is investigated. This effect is avoided in the D-EIT cooling scheme due to the simultaneous cooling of all motional modes of a single $^{40}\text{Ca}^+$ ion. Furthermore, it is shown that off-resonant excitation is a limitation in standard EIT cooling that is overcome in D-EIT cooling enabling higher cooling rates for systems that operate in the Lamb-Dicke regime. Finally, the GSC performance both in cooling rate and steady-state temperature of D-EIT cooling, standard EIT cooling, and concatenated standard EIT cooling pulses are investigated and compared. The results of the comparison are shown in Table 2.2, listing values for the final steady-state mean motional quantum number n_{ss} and the time t_{ss} needed to reach n_{ss} between the different cooling schemes. These results were obtained for a single-photon blue detuning of $\Delta = 71.5\,\text{MHz}$, which is the maximum blue detuning that could be achieved for both single and D-EIT cooling given the available acousto-optical modulator (AOM) bandwidth.

On the theory side, a detailed thermodynamic interpretation of laser cooling is presented based on an analogy between linear response theory and the Lamb-Dicke regime. Within the Lamb-Dicke regime, a detailed description of the system in the form of an analytical theory for both single EIT and D-EIT cooling is given. A theory for time-dependent rates has been developed to describe the system beyond the Lamb-Dicke regime and this theory has been compared to the measured data.

Contributions

Table 2.3: Author contributions, which are the same for both publications presented in this section.

Name	Research question/plan	Conducting experiments	Evaluation of results	Preparation of the manuscript
Nils Scharnhorst	✓	✓	✓	✓
Javier Cerrillo Moreno[a]	✓		✓	✓
Johannes Kramer		✓		✓
Ian D. Leroux	✓			✓
Jannes B. Wübbena	✓			✓
Alex Retzker				✓
Piet O. Schmidt	✓		✓	✓

[a] Contributed the theoretical analysis and simulation of the experimental data.

2.3 Uncertainties in the aluminum clock

The experimental results obtained in the course of this work lead to estimates of some systematic effects that shift the $^{27}\text{Al}^+$ clock transition from its ideal unperturbed frequency and thus contribute to the error budget of an $^{27}\text{Al}^+/^{40}\text{Ca}^+$ quantum logic clock.

2.3.1 Black-body radiation shift

The experiment is conducted at room temperature. As a consequence, thermal blackbody radiation (BBR) couples to the electronic level-structure of trapped ions. In particular, BBR shifts the ground ($^1\text{S}_0$) and excited state ($^3\text{P}_0$) of the clock transition in $^{27}\text{Al}^+$ differently, thus making the clock transition frequency depend on the temperature of the environment as seen by the clock ion.

Rosenband at al. [55] give the derivation for the calculation of the BBR shift as a function of the temperature $T \pm \Delta T$, where T is the temperature seen by the trapped clock ion and ΔT the uncertainty on that temperature. Following [55], the fractional BBR shift is calculated as

$$\frac{\Delta\nu_{\text{BBR}}}{\nu} = \frac{\pi(k_{\text{B}}T)^4 \Delta\alpha(0)}{60\epsilon_0 \hbar^4 c^3 \nu}, \tag{2.1}$$

where k_{B} is the Boltzmann constant, ϵ_0 the vacuum permittivity, c the vacuum speed of light, and $\Delta\alpha(0)$ the static differential polarizability of the $^1\text{S}_0$ to $^3\text{P}_0$ clock transition in $^{27}\text{Al}^+$. In principle, the BBR shift depends on the average of the dynamic polarizability, weighted by the blackbody spectrum. But in $^{27}\text{Al}^+$, all relevant transitions are in the deep UV such that the differential polarizability at infrared wavelengths that make up the room-temperature BBR spectrum are close to the DC (static) value. Making this approximation is justified by our limited knowledge of the differential polarizability and thus, the static differential polarizability may be used without loss of accuracy. For $\Delta\alpha(0)$ a value of $(0.82 \pm 0.08) \times 10^{-41}\,\text{J}\,\text{m}^2\,\text{V}^{-2}$ has been calculated by Safronova et al. [56]. Assuming a room temperature of $(300.0 \pm 0.5)\,\text{K}$, the BBR shift is calculated to be $(-3.8 \pm 0.4) \times 10^{-18}$.

Figure 2.3 displays the uncertainty of the fractional BBR shift as a function of ΔT. The main contribution to ΔT arises from insufficient knowledge of the BBR emitted from the surfaces of the trap toward the position of the clock ion. Typically, the trap surfaces are heated above room temperature by the rf power applied to the rf electrodes for the generation of the radial confinement of the ion. As shown in [57], ΔT for the
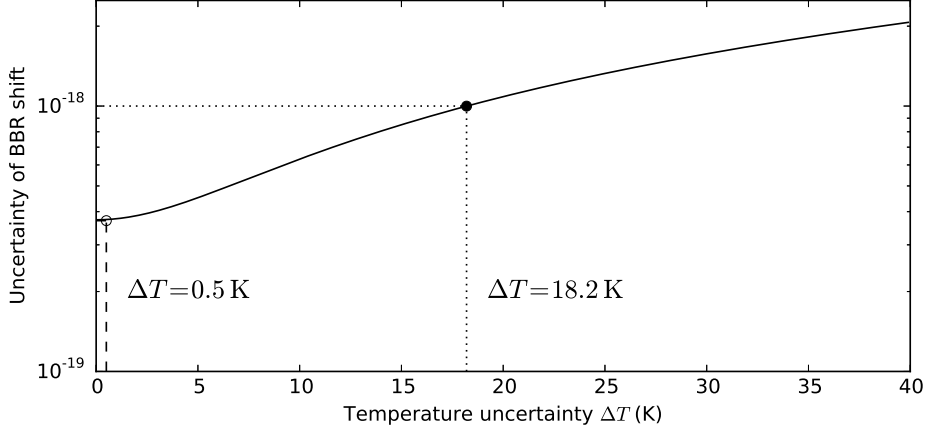
Figure 2.3: Uncertainty of the fractional BBR shift as a function of the uncertainty ΔT of the temperature seen by the clock ion (solid line). The dashed lines show the measured case of $\Delta T = 0.5$ K, while the dotted lines indicate $\Delta T = 18.2$ K, for which the uncertainty of the fractional BBR shift crosses 1×10^{-18}. The uncertainty of the BBR shift at $\Delta T = 0$ K results from the uncertainty attributed to the differential scalar polarizability [56].

trap geometry used in this work has been evaluated to be 0.5 K at the position of the trapped ion. The uncertainty of the BBR shift is dominated by the uncertainty of the differential polarizability such that the contribution of ΔT is negligible.

2.3.2 Second order Doppler shift due to excess micromotion

A displacement of a trapped ion from the rf node of a Paul trap or a phase difference between the ac potentials on the electrodes results in a driven motion of the ion due to the ac-field at the ion's location. This motion is called excess micromotion (EMM). EMM due to a displacement of the ion can be compensated by applying static electric fields that push the ion back onto the rf node. In the case of a phase difference between the ac potentials, a fraction of the ac potential can be fed to the direct current (DC) electrodes of the trap, in order to compensate the EMM. Residual EMM causes a second order Doppler shift, which contributes to the error budget of the clock. Following [58], the second order fractional Doppler shift $\frac{\Delta \nu_{EMM}}{\nu}$ on the $^{27}\text{Al}^+$ clock transition ν due to EMM can be expressed as

$$\frac{\Delta \nu_{\text{EMM}}(z)}{\nu} = -\frac{1}{2c^2} \sum_{i=x,y,z} v_{\text{i}}^2(z), \tag{2.2}$$

where c is the vacuum speed of light, and $v_{\text{i}}(z)$ the EMM induced velocity of the ion along axis i at location z on the trap axis. The velocities v_{i} can be calculated from the
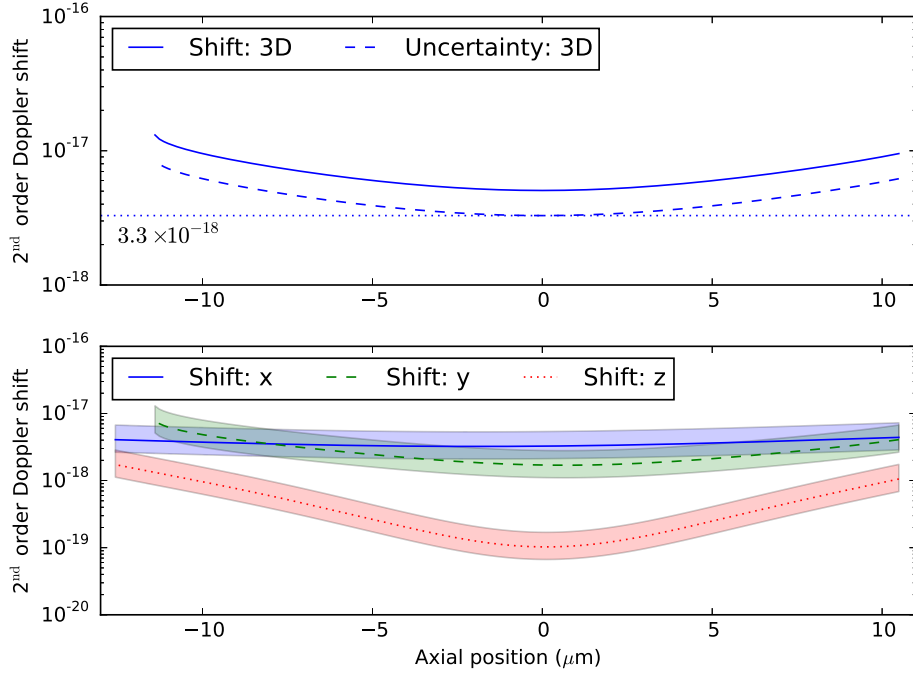
Figure 2.4: Fractional second order Doppler shift on the ^{27}Al$^+$ clock ion caused by residual EMM as a function of the location of the clock ion on the trap axis z. (Top panel) The solid line represents the overall fractional shift and the dashed line corresponds to 65 % of the fractional shift, which is the attributed uncertainty due to measurement uncertainties of the Rabi frequency of carrier and EMM sideband Rabi flops. (Bottom panel) Fractional EMM shifts along the individual axis, which together result in the 3D EMM shift shown in the top panel. The shaded areas represent the uncertainty, dominated by the measurement uncertainty of the Rabi frequency on the micromotion sideband. z: horizontal trap axis, x: horizontal and perpendicular to the trap axis, and y: vertical and perpendicular to the trap axis.

measured Rabi frequencies of a Rabi flop on a carrier transition $f_{\mathrm{Car}}(z)$ and micromotion sideband $f_{\mathrm{MM}}(z)$ as

$$v_{\mathrm{i}}(z) = \frac{\sqrt{2}\,\Omega}{k_{729}} \frac{f_{\mathrm{MM,i}}(z)}{f_{\mathrm{Car,i}}(z)} \frac{m_{\mathrm{Ca}}}{m_{\mathrm{Al}}}, \tag{2.3}$$

where $\Omega = 28.209\,\mathrm{MHz}$ is the frequency of the radially confining rf quadrupole field, and k_{729} is the wave vector of the $^2\mathrm{S}_{1/2}$ to $^2\mathrm{D}_{5/2}$ logic transition in $^{40}\mathrm{Ca}^+$. The ratio of the masses of the calcium m_{Ca} and aluminum ion m_{Al} in Equation 2.3 extrapolates the velocities obtained from measurements of $f_{\mathrm{MM}}(z)$ and $f_{\mathrm{Car}}(z)$ on a $^{40}\mathrm{Ca}^+$ ion to the velocities of the $^{27}\mathrm{Al}^+$ ion at position z on the trap axis.

In this experiment, EMM is first coarsely minimized with the correlation technique [58, 59]. In a second step, the resolved sideband method [58, 59] is iteratively employed on three non-coplanar directions for further minimization. Here, the EMM is measured

and minimized on the 729 nm logic transition of a single trapped ^{40}Ca$^+$ ion. After optimization, the measurements of the residual EMM are combined and converted to an overall EMM induced second order Doppler shift for a ^{40}Ca$^+$ ion as a function of the ion's position around the EMM minimum along the trap axis. By weighting the results from the single ^{40}Ca$^+$ ion measurements with the mass ratio between ^{40}Ca$^+$ and ^{27}Al$^+$, one obtains the EMM-caused second order Doppler shift of the ^{27}Al$^+$ clock ion. A typical experimental result of such a measurement run is displayed in Figure 2.4. The top panel shows the overall fractional EMM shift, together with an attributed measurement uncertainty of 65 % based on the uncertainty of the Rabi frequencies $f_{Car}(z)$ and $f_{MM}(z)$. Here, the uncertainty of $f_{MM}(z)$ dominates the uncertainty of the EMM shift. Rabi flops on micromotion sidebands have smaller Rabi frequencies than carrier Rabi flops and therefore a lower contrast due to dephasing effects from external fields and phase noise of the interrogating laser. As a consequence, the uncertainty of $f_{MM}(z)$ is large compared to $f_{Car}(z)$. The bottom panel of Figure 2.4 shows the EMM shift along individual Cartesian axes, which together result in the overall EMM shift displayed in the top panel.

At the location of minimum EMM, the resulting shift is $(-5.1 \pm 3.3) \times 10^{-18}$. For the motional trap frequencies in the setup, the ion-to-ion distance in a ^{27}Al$^+$/^{40}Ca$^+$ two-ion crystal oriented along the trap axis is around 4 µm. As can be seen from Figure 2.4, the curvature of the shift around its minimum is small enough that displacing the ion a few micrometers away from the trap center will not increase the uncertainty of the shift by more than 2×10^{-19}.

2.3.3 ac-Stark shift due to cooling lasers and time-dilation shift

The finite temperature of a trapped ion is associated with non-zero kinetic energy E_k and the ion's motion results in a second order Doppler shift, referred to as time-dilation shift. It has to be noted, that this shift never vanishes for a trapped particle, even at 100 % motional ground state population, due to the zero-point energy.

Time-dilation shift

The derivation of the time-dilation shift $\frac{\Delta\nu_{sec}}{\nu}$ presented in this subsection follows [23]. It is simulated for a ^{27}Al$^+$ clock ion in an ^{27}Al$^+$/^{40}Ca$^+$ two-ion crystal and can be written as

$$\frac{\Delta\nu_{sec}}{\nu} = -\frac{\hbar(\bar{n}+1/2)}{2m_{Al}c^2}\sum_i \omega_i(1+S_i), \tag{2.4}$$

where $\bar{n}$ is the mean-motional quantum number. ω_i is the frequency of mode i, m_{Al} the mass of an aluminum ion, and S_i is a scaling factor representing the contribution of intrinsic micromotion [58] to the time-dilation shift. The numerator in Equation 2.4 – including the sum – is the total energy in the set of harmonic oscillators. By the equipartition theorem, half of the total energy corresponds to the kinetic energy of the trapped $^{27}Al^+$ ion, resulting in the factor two in the denominator of Equation 2.4 to get the kinetic energy, which is then compared to the the rest energy $m_{Al}c^2$. For the radial modes, the scaling factor is calculated as

$$S_i = \frac{2\epsilon^2/\mu}{2\epsilon^2/\mu - 2\alpha - (1 - \sqrt{\mu}b_{Ca}/b_{Al})}, \tag{2.5}$$

and for the axial modes as $S_i = b_{Al}^2$. Here, $0 \leq \alpha \leq 1$ is a unitless radial geometry factor. For the simulation α is set to $1/2$, corresponding to perfect symmetry of the radial trapping potential, which is justified by the almost degenerate radial mode frequencies. $\mu = m_{Al}/m_{Ca}$ is the mass ratio of the clock and logic ion and

$$\epsilon = \frac{\sqrt{\omega_{radial}^2 + \frac{\omega_{axial}^2}{2}}}{\omega_{axial}} \tag{2.6}$$

corresponds to the ratio of the ponderomotive and axial mode frequency. The motional amplitudes b_{Al} of the $^{27}Al^+$ clock and b_{Ca} of the $^{40}Ca^+$ logic ion are given as

$$b_{Ca} = \sqrt{\frac{\mu - \mu^2 + \epsilon^2(\mu^2 - 1) + a}{2a}}, \qquad b_{Al} = \sqrt{1 - b_{Ca}^2}, \tag{2.7}$$

with

$$a = \sqrt{\epsilon^4(\mu^2 - 1) - 2\epsilon^2(\mu - 1)^2\mu(1 + \mu) + \mu^2(1 + (1 - \mu)\mu)}. \tag{2.8}$$

It is assumed that all motional modes are cooled to the same mean-motional quantum number $\bar{n}$. In the following, the results are simulated for two different sets of motional mode frequencies of the two-ion crystal. One set describes the settings that have been used in the experimental setup up to the time of writing ("Current"), the other set of mode frequencies corresponds to experimental trapping parameters, for which all six modes bunch around two frequencies ("Bunching"). Table 2.4 lists the mode frequencies within each set. Figure 2.5 displays the time-dilation shift as a function of $\bar{n}$ of the six modes of a $^{27}Al^+/^{40}Ca^+$ two-ion crystal. The $\bar{n}$ has an attributed measurement uncertainty of 10% and which is assumed to be the same for all modes. For the "Bunching"("Current") mode frequency set, an $\bar{n} = 7.8$ ($\bar{n} = 5$) results in an uncertainty of the time-dilation shift of 1×10^{-18}. For both mode frequency sets, the contribution of the intrinsic micromotion to the time-dilation shift is about equal to the contribution of the kinetic energy. Due to the zero-point energy, the time-dilation shift is non-zero

Table 2.4: Sets of mode frequencies used to simulate time-dilation shifts.

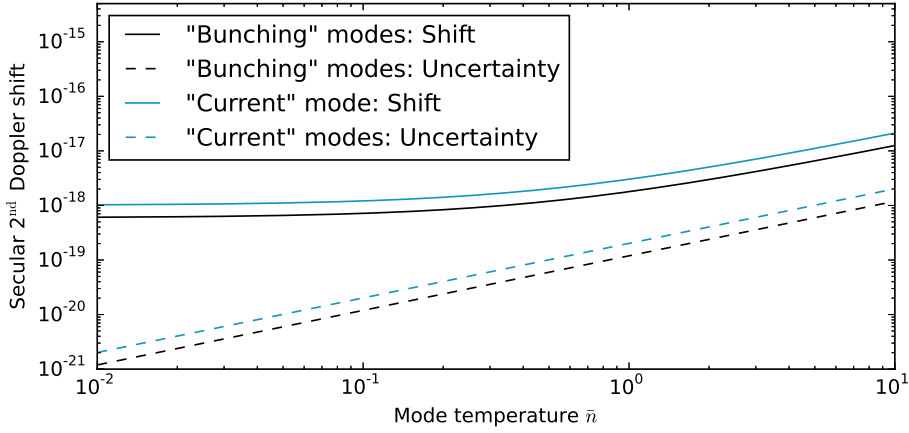| Mode i	$\omega_{\text{Bunching,i}}$ in (MHz)	$\omega_{\text{Current,i}}$ in (MHz)
Axial in-phase	0.925	0.978
Axial out-of-phase	1.775	1.762
Radial in-phase 1	0.925	2.458
Radial in-phase 2	0.925	2.458
Radial out-of-phase 1	1.775	3.743
Radial out-of-phase 2	1.775	3.743

Figure 2.5: Time-dilation shift as a function of $\bar{n}$ of the six modes of a $^{27}\text{Al}^+/^{40}\text{Ca}^+$ two-ion crystal. All modes are assumed to have the same $\bar{n}$. Solid lines represent the time-dilation shift and the dashed lines the corresponding uncertainties, which are dominated by the 10 % measurement uncertainty for the $\bar{n}$. The blue lines show the results for the set of "Current" and the black lines those of the "Bunching" mode frequencies.

at $\bar{n} = 0$ and is simulated to 6×10^{-19} (1×10^{-18}) for the "Bunching"("Current") mode frequency set, with negligible uncertainty.

It is worth pointing out that the time-dilation shift depends only on the velocity, i.e. the kinetic energy of the ion in the lab frame, which is equivalent to the thermal energy E_{th} of the ion. For a given E_{th}, the conserved quantity is $E_{\text{th}} \propto \omega\bar{n}$ up to constant scaling factors. Therefore, for the same E_{th}, the larger "Current" mode frequencies yield a lower $\bar{n}$ compared to the smaller "Bunching" mode frequencies. If Figure 2.5 was plotted against E_{th} rather than $\bar{n}$, the curves would collapse into a single line independent of trap parameters. In any case, as mentioned in [53], Doppler cooling is insufficient to reach those temperatures.

In order to achieve sub-Doppler temperatures, GSC has to applied to the logic ion. Here,

there are two options, GSC of the ion during the clock interrogation, and GSC before the clock interrogation.

Interrogation time limit due to background heating rates

To avoid any influence of the cooling lasers on the clock transition, the ions can be cooled close to the motional ground state before the clock interrogation. Here, based on [28, 29], D-EIT should allow all modes of the $^{27}\text{Al}^+/^{40}\text{Ca}^+$ two-ion crystal to be prepared with $\bar{n} \leq 0.2$. Switching off the cooling lasers during the clock interrogation avoids any laser-induced ac-Stark shift. However, without cooling, the background heating rate will heat the modes up, which increases the time-dilation shift and limits the maximum interrogation time. In the setup, a radial heating rate of $(28.2 \pm 3.4)\,\text{s}^{-1}$, and an axial heating rate of $(45.0 \pm 2.8)\,\text{s}^{-1}$ are typically observed for a single $^{40}\text{Ca}^+$ ion with radial mode frequencies at $2.552\,\text{MHz}$ and $2.540\,\text{MHz}$, and an axial mode frequency of $904.6\,\text{kHz}$. The simulation assumes the measured background heating rate for both sets of mode frequencies. However, due to electronic flicker and random walk frequency noise in the setup, the background heating rate is likely to increase with smaller mode frequencies. As a result, higher heating rates are expected for the "Bunching" mode frequencies compared to the single $^{40}\text{Ca}^+$ ion and "Current" set of mode frequencies. Figure 2.6 illustrates the effect of that background heating rate by showing the time-dilation shift as a function of the clock interrogation time. With the measured uncertainties of the heating rates, an uncertainty on the time-dilation shift of 1×10^{-18} is reached at $0.16\,\text{s}$ ($0.29\,\text{s}$) for the "Current" ("Bunching") set of mode frequencies. This time can be extended by measuring the heating rate more precisely to allow a better prediction of the evolving ion temperature and time-dilation shift during the interrogation.

ac-Stark shift of cooling lasers

The alternative to GSC prior to the clock interrogation is GSC during the clock interrogation. This has the advantage of a constant temperature of the ion and the interrogation time is not limited due to background heating rates. However, the cooling lasers cause an ac-Stark shift of the clock transition and therefore contribute to the error budget of the clock. Assuming GSC via D-EIT cooling (see Section 2.2), the main contribution to the ac-Stark shift is caused by the pump lasers. For a chosen blue detuning Δ, the Rabi frequency of the pump laser is fixed by the requirement to Stark-shift the cooling bright state into resonance with the motional RSB. Consequently, the highest mode frequency of a set of modes determines the dominant intensity and therefore the ac-Stark shift on the clock transition. The required Rabi frequency of the pump laser decreases with
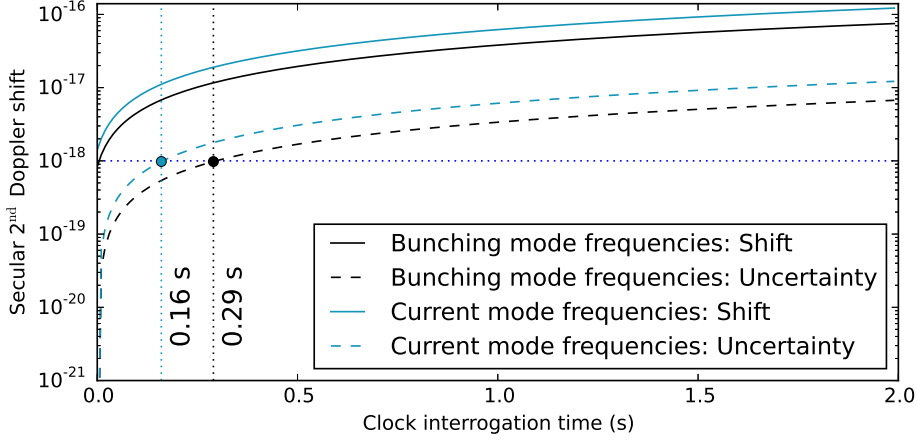
Figure 2.6: Time-dilation shift as a function of the clock interrogation time for the measured background heating rates of $(28.2 \pm 3.4)\,\mathrm{s}^{-1}$ in the radial, and $(45.0 \pm 2.8)\,\mathrm{s}^{-1}$ in the axial direction and an initial $\bar{n}(0) = 0.2$. For both mode frequency sets, the solid lines give the time-dilation shift and the dashed lines the corresponding uncertainty, which is dominated by the uncertainty of the heating rates. For each set the dashed lines mark the clock interrogation time for which the uncertainty of the time-dilation shift is 1×10^{-18}.

Table 2.5: Fractional ac-Stark shift induced by D-EIT cooling beams during clock interrogation. For two different blue detunings Δ, the corresponding Rabi frequencies of the cooling beams are given and the resulting ac-Stark shift.

Detuning Δ (MHz)	Ω_{866} (MHz)	Ω_σ (MHz)	Ω_π (MHz)	ac-Stark shift (10^{-18})
11.3	2	9.34	1.58	-0.2 ± 0.4
72.3	24.5	18.5	8.39	-1.1 ± 5.3

smaller Δ, which also result in higher $\bar{n}$ [29]. This can be tolerated as long as $\bar{n} \leq 7.8$ ($\bar{n} \leq 5$) for the "Bunching"("Current") mode frequency set.

Table 2.5 shows the fractional ac-Stark shift induced by D-EIT cooling beams during clock interrogation. The ac-Stark shift is calculated for $\Delta = 11.3\,\mathrm{MHz}$ and $\Delta = 72.3\,\mathrm{MHz}$. The former is the smallest Δ measured within this work and resulted in $\bar{n} < 5$ for all modes of a trapped single ${}^{40}\mathrm{Ca}^+$ ion with $904.6\,\mathrm{kHz}$ axial, and around $2.55\,\mathrm{MHz}$ radial mode frequencies. The latter is measured for the largest Δ during D-EIT cooling investigated within this work and resulted in $\bar{n} < 0.2$ for all modes.

The simulation of the ac-Stark shift follows [55] and the data for the oscillator strengths and transition frequencies is obtained from [60]. The transition dipole matrix element from [61] is used for conversion of the $397\,\mathrm{nm}$ Rabi frequencies into the electric field amplitude. In case of the $866\,\mathrm{nm}$, the dipole matrix element is calculated from the

Table 2.6: Error budget contributions of the $^{27}\text{Al}^+/^{40}\text{Ca}^+$ quantum logic optical clock due to systematic effects discussed in this section. The values represent the case of D-EIT cooling of all "Bunching" modes during the clock interrogation at a blue detuning of 11.3 MHz. Shifts and uncertainties are given in fractional frequency units.

Effect	Shift (10^{-18})	Uncertainty (10^{-18})
Black-body radiation shift	-3.8	0.4
Excess micromotion shift	-5.1	3.3
Time-dilation shift[a]	-4.2	0.4
ac-Stark shift	-0.2	0.4

[a] Assuming D-EIT cooling of all modes to $\bar{n} = 3.0 \pm 0.3$ during the clock interrogation.

Einstein A coefficient given in [60]. For all measured Rabi frequencies an uncertainty of 30 % is assumed. In all cases, the shift uncertainty is larger than the shift itself, because the oscillator strengths for the relevant transitions in $^{27}\text{Al}^+$ are not yet accurately known [55]. According to the simulations, D-EIT cooling at small Δ is tolerable during clock operation.

2.3.4 Error budget contributions of the $^{27}\text{Al}^+/^{40}\text{Ca}^+$ quantum logic optical clock

The results of this section form part of the error budget of an $^{27}\text{Al}^+/^{40}\text{Ca}^+$ quantum logic optical clock. Table 2.6 summarizes the shift and its associated uncertainty of the $^{27}\text{Al}^+$ clock transition from its ideal unperturbed frequency for the effects discussed in this section. The values represent the case of D-EIT cooling of all "Bunching" modes (see Table 2.4) to $\bar{n} = 3$ during the clock interrogation at a blue detuning of 11.3 MHz. Due to the cooling, the maximum clock interrogation time is not limited by background heating rates. Longer clock interrogation times potentially yield a higher clock stability, which is the advantage of this configuration.

3 Summary and Outlook

Summary

Within this thesis, a high-bandwidth transfer-lock scheme has been developed and demonstrated, which is capable of transferring short-term stability from a stable master laser to a laser at 729 nm with no pre-stabilization, via a frequency comb [24]. The scheme synthesizes a virtual beat signal between the 729 nm and a stable master laser, suppressing the effect of the comb noise by microwave feed-forward electronics. Such a transfer-oscillator lock [32] relaxes the requirements for the comb lock. By eliminating the need for auxiliary reference cavities for laser pre-stabilization at each wavelength, this capability allows a substantial simplification of experimental setups requiring multiple stable lasers.

The transfer-locking scheme allows one to phase-lock lasers at different wavelengths to the same master laser. As a consequence, all those lasers are also phase-stable with respect to each other. Standard techniques for phase-locks, such as transfer cavities, cannot bridge large wavelength differences due to limited bandwidth of mirror coatings. The novel ability to phase-lock spectrally separated lasers is particularly important for the Doppler cooling laser at 397 nm and its repumper at 866 nm - phase stability between them is critical for the realization of the double bright EIT cooling scheme described in [28, 29].

The transfer-locking scheme enabled the first experimental implementation of a variant of double EIT cooling [28, 29]. Double bright EIT cooling (D-EIT) has been developed in the context of this thesis as an approach for fast, multi-mode ground state cooling for well-separated motional frequencies. Standard single EIT cooling only allows for ground state cooling of modes within the the narrow frequency range of its cooling resonance. Furthermore, for high cooling rates it suffers from off-resonant excitation via unused excited states and the detrimental effect of hot spectator modes, which increase the minimum achievable mean motional quantum number with increasing cooling rate [29]. In contrast to the original theory proposals for double EIT [62], the D-EIT scheme incorporates all relevant excited states in its level scheme and therefore solves the problem

of off-resonant scattering. Applying the repumper and Doppler cooling lasers in D-EIT configuration, one dark state and two individually shiftable bright dressed states are created. The bright states can be brought into resonance with different RSB of different motional mode frequencies of a trapped ion. This allows ground state cooling of all three motional degrees of freedom of a single $^{40}\text{Ca}^+$ ion within a single cooling pulse, as demonstrated in [28].

A comparison between the results of D-EIT cooling and simulations [29] also serves as a benchmark of the quality of the transfer-locking scheme. Decoherence between repumper and the Doppler cooling beams would limit the lifetime of the dark state during D-EIT cooling and allow for carrier scattering and consequent recoil heating. However, the measured temperatures in D-EIT agree with the simulations which assume perfect coherence between the laser fields, indicating a high mutual phase-stability between the 866 nm and 397 nm lasers.

Finally, estimates of the fractional systematic shifts and their uncertainties for a projected $^{27}\text{Al}^+/^{40}\text{Ca}^+$ quantum logic clock are given, based on measurement results obtained in the course of this thesis. It is shown that the BBR shift of $(-3.8 \pm 0.4) \times 10^{-18}$ will not impose any limitation on the error budget for an $^{27}\text{Al}^+/^{40}\text{Ca}^+$ quantum logic clock. The shift due to EMM of $(-5.1 \pm 3.3) \times 10^{-18}$ as well as its uncertainty might be reduced in further optimization runs. Since the EMM is relatively uniform around the location of its minimum along the trap axis, a two-ion crystal is not expected to experience significantly more EMM than a single ion. The uncertainty of time-dilation shift due to residual motion of the clock ion stays below -1×10^{-18} as long as the motional modes are cooled to $\bar{n} < 5$, which requires cooling below the Doppler cooling limit. GSC with D-EIT cooling during the clock interrogation is expected to result in a fractional ac-Stark shift of $(-0.2 \pm 0.4) \times 10^{-18}$ for a small blue detuning, where all modes are expected to fulfill $\bar{n} < 5$. Alternatively, if all six modes of the two-ion crystal are cooled to $\bar{n} = 0.2$ before the clock interrogation with no cooling during the interrogation itself, the maximum clock time is limited by the background heating rate, whose uncertainty dominates the time-dilation shift. With the measured values of the heating rates, the clock interrogation time is limited to <300 ms if the uncertainty of the time-dilation shift is required to be below -1×10^{-18}.

Outlook for future work

In contrast to a single trapped ion, a $^{27}\text{Al}^+/^{40}\text{Ca}^+$ crystal has six motional degrees of freedom. Due to the mass ratio of $^{27}\text{Al}^+$ to $^{40}\text{Ca}^+$, an amplitude of the trapping quadrupole field can be identified for which all six modes bunch around just two fre-

quencies. Providing two individually shiftable bright states, the D-EIT scheme allows cooling of all modes of the two-ion crystal within a single cooling pulse. This requires, however, that every D-EIT cooling beam has a projection on the axial and both radial modes. This is not the case in the current beam geometry [29], but may be achieved, e.g. by rotating the trap by 45° in the horizontal plane with respect to the laser beams and magnetic field. Furthermore, the D-EIT cooling scheme allows even triple-EIT cooling [62], where a second dark state at the position of a motional blue sideband (BSB) suppresses all leading-order heating processes on that mode. Triple-EIT cooling of a certain mode can be attained, if the magnetic field strength is chosen such that the 866 nm $\sigma^{\pm}$ polarized laser is red detuned by the respective mode frequency from a transition connecting an additional $^2\mathrm{D}_{3/2}$ sublevel to the $\mathrm{P}_{\pm}^v$ virtual level.

D-EIT cooling relies on the relative phase stability among the cooling lasers which is realized by the transfer-locking scheme [24]. The maximum bandwidth for relative phase-stability is limited by the intrinsic noise of the frequency comb, whose reduction would thus result in a longer lived dark state, higher cooling rates, and lower steady-state mean motional quantum numbers after D-EIT cooling. Thanks to continued progress in the development of frequency combs, all-fiber master oscillators are now available, which have been reported to be quieter than master oscillator in the frequency comb used in this work. Thus, a replacement of the current master oscillator might improve D-EIT cooling as well as reduce the phase noise of the transfer-locked lasers.

Apart from laser phase noise, external magnetic field noise has a detrimental effect on the coherence between atomic transitions of the ion and the interrogating laser field(s). External magnetic field noise is suppressed by an active magnetic field compensation in the setup [29]. However, its suppression bandwidth is limited to <100 Hz due to the inductance of the compensation coils. An (additional) passive shield made of μ-metal and aluminum around the vacuum chamber would yield a overall better suppression of external magnetic field noise.

The typical lifetime of an $^{27}\mathrm{Al}^+/^{40}\mathrm{Ca}^+$ crystal in the setup is less than five hours. It is mainly limited by the reaction of the trapped $^{27}\mathrm{Al}^+$ with residual hydrogen in the vacuum chamber to form AlH^+. For longer measurement campaigns of the $^{27}\mathrm{Al}^+/^{40}\mathrm{Ca}^+$ quantum logic optical clock it would be beneficial to either improve the lifetime of the two-ion crystal by reducing the amount of reactive background gas in the vacuum chamber, or to be able to re-load a new $^{27}\mathrm{Al}^+/^{40}\mathrm{Ca}^+$ crystal with minimum dead-time for the experiment. Prolonging the lifetime requires extensive work on the vacuum system. Loading of an $^{27}\mathrm{Al}^+$ ion in the setup commonly takes 2−20 min. The dead time due to re-loading of an $^{27}\mathrm{Al}^+/^{40}\mathrm{Ca}^+$ crystal in our setup is limited by the time required to sympathetically cool the $^{27}\mathrm{Al}^+$ ion after ablation loading. The neutral aluminum atoms have large residual velocities after being ablated and ionized, which renders sympathetic

cooling inefficient due to the initially small motional coupling between the ^{40}Ca$^+$ logic and ^{27}Al$^+$ clock ion [63]. A reduction of this dead-time could be achieved by selective ionization only of the lowest velocity class in the aluminum atom beam. The atom beam is generated underneath the trap center by an ablation laser from an aluminum target [29], while the ionization laser beam currently runs along the trap axis, perpendicular to the neutral atom beam. In this geometry, a spectral selection of a velocity class by tuning the frequency of the ionization laser is almost impossible. If instead the ionization laser were to be aligned parallel to the atom beam the frequency of the ionization resonance would be maximally sensitive to atomic velocity, allowing selective ionization of low-energy atoms. This preferable geometry may be e.g. approximated by sending the aluminum ionization laser from above the trap through the imaging optics for fluorescence detection. Alternatively, a temporal delay between the ablation pulse and switching on of the ionization pulse can help to select slower atoms. However, given the short distance of approximately $2\,\mathrm{cm}$ between the aluminum ablation target and the trap center and the large thermal velocities around $5\,\mathrm{km\,s^{-1}}$ [63], such time-of-flight discrimination requires a control of the delay on the level of nanoseconds which is similar to the pulse length of the ablation laser.

During the work for this thesis preliminary experiments toward quantum-logic spectroscopy of ^{27}Al$^+$/^{40}Ca$^+$ crystals were conducted. Fig. 3.1 shows the results of first spectroscopy experiments on the $^1S_0$ to $^3P_1$ logic transition in aluminum. Once stable laser power at $267\,\mathrm{nm}$ is available, all ingredients for the aluminum clock will be at hand.
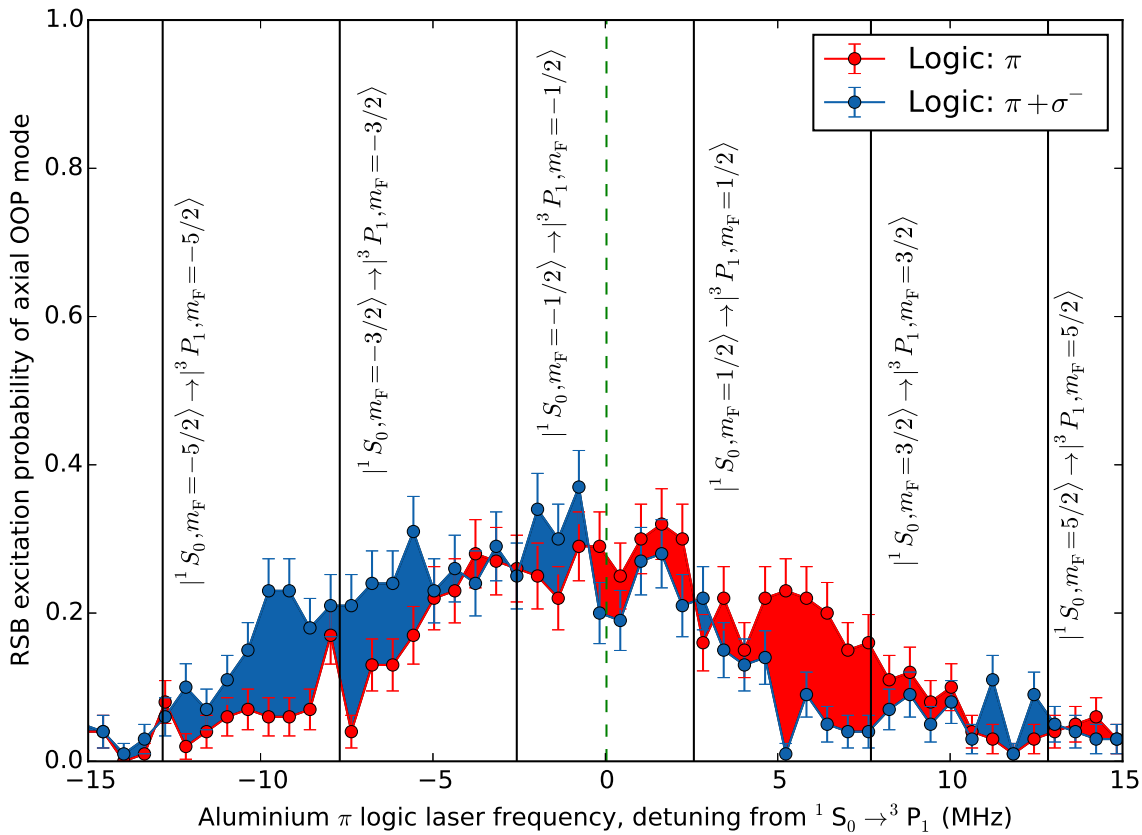
Figure 3.1: Excitation probability on the axial red side band (RSB) of the out-of-phase (OOP) mode of an $^{27}\text{Al}^+/^{40}\text{Ca}^+$ crystal after ground state cooling followed by 1 ms of illumination with either the aluminum logic π beam (red data points) or the combined π and σ^- beams (blue data points). The logic σ^- beam is tuned to the unperturbed $^1S_0 \rightarrow\,^3P_1$ resonance (dashed vertical line). Solid vertical lines indicate theoretical transition frequencies accessible with the logic π beam, for the measured magnetic field of 4.165 G. When the strong aluminum logic beams are in resonance with a logic transition, they heat the aluminum ion, which in turn sympathetically heats the calcium ion via the Coulomb coupling. Directly after ground state cooling the RSB excitation probability of that mode is close to zero. Due to the heating of the logic beams the OOP mode becomes hotter and scattering on its RSB increases with its temperature. Just applying the logic π beam results in a symmetric RSB excitation with respect to zero detuning. After applying the logic π and σ^- laser together, the excitation spectrum becomes asymmetric. This indicates, that population is transferred from positive (red area) to negative (blue area) Zeeman states, demonstrating optical pumping on the aluminum logic transition by the logic σ^- beam.

Bibliography

[1] Bureau International des Poids at Mesures. *The International System of Units (SI)*. Organisation Intergouvernementale de la Convention du Métre, 2006. [Cited on page 11.]

[2] BIPM. Draft of the ninth SI Brochure, 10 2016. [Cited on pages 11 and 12.]

[3] Theodor W. Hänsch. Passion for precision. *Nobel Lecture*, 2005. [Cited on pages 11 and 12.]

[4] Patrick Gill. When should we change the definition of the second? *Philosophical Transactions of the Royal Society of London A: Mathematical, Physical and Engineering Sciences*, 369(1953):4109–4130, 2011. [Cited on page 12.]

[5] B. J. Bloom, T. L. Nicholson, J. R. Williams, S. L. Campbell, M. Bishof, X. Zhang, W. Zhang, S. L. Bromley, and J. Ye. An optical lattice clock with accuracy and stability at the 10-18 level. *Nature*, 506(7486):71–75, February 2014. [Cited on page 12.]

[6] N. Huntemann, C. Sanner, B. Lipphardt, Chr. Tamm, and E. Peik. Single-ion atomic clock with 3×10^{-18} systematic uncertainty. *Phys. Rev. Lett.*, 116:063001, Feb 2016. [Cited on page 12.]

[7] S. Bize, S. Diddams, U. Tanaka, C. Tanner, W. Oskay, R. Drullinger, T. Parker, T. Heavner, S. Jefferts, L. Hollberg, W. Itano, and J. Bergquist. Testing the Stability of Fundamental Constants with the Hg+199 Single-Ion Optical Clock. *Physical Review Letters*, 90(15), April 2003. [Cited on page 12.]

[8] M. Fischer, N. Kolachevsky, M. Zimmermann, R. Holzwarth, Th. Udem, T. W. Hänsch, M. Abgrall, J. Grünert, I. Maksimovic, S. Bize, H. Marion, F. Pereira Dos Santos, P. Lemonde, G. Santarelli, P. Laurent, A. Clairon, C. Salomon, M. Haas, U. D. Jentschura, and C. H. Keitel. New limits on the drift of fundamental constants from laboratory measurements. *Phys. Rev. Lett.*, 92:230802, Jun 2004. [Cited on page 12.]

[9] S. Blatt, A. D. Ludlow, G. K. Campbell, J. W. Thomsen, T. Zelevinsky, M. M. Boyd, J. Ye, X. Baillard, M. Fouché, R. Le Targat, A. Brusch, P. Lemonde, M. Takamoto, F.-L. Hong, H. Katori, and V. V. Flambaum. New limits on coupling of fundamental constants to gravity using ^{87}Sr optical lattice clocks. *Phys. Rev. Lett.*, 100:140801, Apr 2008. [Cited on page 12.]

[10] T. Rosenband, D. B. Hume, P. O. Schmidt, C. W. Chou, A. Brusch, L. Lorini, W. H. Oskay, R. E. Drullinger, T. M. Fortier, J. E. Stalnaker, S. A. Diddams, W. C. Swann, N. R. Newbury, W. M. Itano, D. J. Wineland, and J. C. Bergquist. Frequency ratio of Al$^+$ and Hg$^+$ Single-Ion Optical Clocks; Metrology at the 17th Decimal Place. *Science*, 319(5871):1808–1812, 2008. [Cited on pages 12 and 17.]

[11] R. M. Godun, P. B. R. Nisbet-Jones, J. M. Jones, S. A. King, L. A. M. Johnson, H. S. Margolis, K. Szymaniec, S. N. Lea, K. Bongs, and P. Gill. Frequency ratio of two optical clock transitions in ^{171}Yb$^+$ and constraints on the time variation of fundamental constants. *Phys. Rev. Lett.*, 113:210801, Nov 2014. [Cited on pages 12 and 17.]

[12] N. Huntemann, B. Lipphardt, Chr. Tamm, V. Gerginov, S. Weyers, and E. Peik. Improved limit on a temporal variation of m_p/m_e from comparisons of Yb$^+$ and Cs atomic clocks. *Phys. Rev. Lett.*, 113:210802, Nov 2014. [Cited on pages 12 and 17.]

[13] M. J. Martin, M. Bishof, M. D. Swallows, X. Zhang, C. Benko, J. von Stecher, A. V. Gorshkov, A. M. Rey, and Jun Ye. A quantum many-body spin system in an optical lattice clock. *Science*, 341(6146):632–636, 2013. [Cited on page 12.]

[14] A.M. Rey, A.V. Gorshkov, C.V. Kraus, M.J. Martin, M. Bishof, M.D. Swallows, X. Zhang, C. Benko, J. Ye, N.D. Lemke, and A.D. Ludlow. Probing many-body interactions in an optical lattice clock. *Annals of Physics*, 340(1):311 – 351, 2014. [Cited on page 12.]

[15] Benjamin M. Roberts, Geoffrey Blewitt, Conner Dailey, Mac Murphy, Maxim Pospelov, Alex Rollings, Jeff Sherman, Wyatt Williams, and Andrei Derevianko. Search for domain wall dark matter with atomic clocks on board global positioning system satellites. *Nature Communications*, 8(1):1195, October 2017. [Cited on page 12.]

[16] Fouad G. Major. *The Quantum Beat: Principles and Applications of Atomic Clocks.* Springer, June 2007. [Cited on page 12.]

[17] Mohinder S. Grewal, Angus P. Andrews, and Chris G. Bartone. *Global Navigation*

Satellite Systems, Inertial Navigation, and Integration. John Wiley & Sons, January 2013. [Cited on page 12.]

[18] M. Vermeer. Chronometric levelling. Reports of the Finnish Geodetic Institute 83(2), Geodeettinen Laitos, Geodetiska Institutet, 1983. [Cited on pages 12 and 17.]

[19] Arne Bjerhammar. On a relativistic geodesy. *Bulletin Géodésique*, 59(3):207–220, September 1985. [Cited on pages 12 and 17.]

[20] C. Lisdat, G. Grosche, N. Quintin, C. Shi, S. M. F. Raupach, C. Grebing, D. Nicolodi, F. Stefani, A. Al-Masoudi, S. Dörscher, S. Häfner, J.-L. Robyr, N. Chiodo, S. Bilicki, E. Bookjans, A. Koczwara, S. Koke, A. Kuhl, F. Wiotte, F. Meynadier, E. Camisard, M. Abgrall, M. Lours, T. Legero, H. Schnatz, U. Sterr, H. Denker, C. Chardonnet, Y. Le Coq, G. Santarelli, A. Amy-Klein, R. Le Targat, J. Lodewyck, O. Lopez, and P.-E. Pottie. A clock network for geodesy and fundamental science. *Nature Communications*, 7:12443, August 2016. [Cited on pages 12 and 17.]

[21] Andrew D. Ludlow, Martin M. Boyd, Jun Ye, E. Peik, and P. O. Schmidt. Optical atomic clocks. *Rev. Mod. Phys.*, 87:637–701, Jun 2015. [Cited on pages 12 and 13.]

[22] P. O. Schmidt, T. Rosenband, C. Langer, W. M. Itano, J. C. Bergquist, and D. J. Wineland. Spectroscopy Using Quantum Logic. *Science*, 309(5735):749–752, July 2005. [Cited on page 13.]

[23] Jannes B. Wübbena, Sana Amairi, Olaf Mandel, and Piet O. Schmidt. Sympathetic cooling of mixed-species two-ion crystals for precision spectroscopy. *Phys. Rev. A*, 85(4):043412, April 2012. [Cited on pages 13 and 27.]

[24] Nils Scharnhorst, Jannes B. Wübbena, Stephan Hannig, Kornelius Jakobsen, Johannes Kramer, Ian D. Leroux, and Piet O. Schmidt. High-bandwidth transfer of phase stability through a fiber frequency comb. *Optics Express*, 23(15):19771–19776, July 2015. [Cited on pages 13, 15, 33, and 35.]

[25] E. Riedle, S. H. Ashworth, J. T. Farrell Jr, and D. J. Nesbitt. Stabilization and precise calibration of a continuous-wave difference frequency spectrometer by use of a simple transfer cavity. *Review of Scientific Instruments*, 65(1):42–48, January 1994. [Cited on pages 13 and 18.]

[26] T. Leopold, L. Schmöger, S. Feuchtenbeiner, C. Grebing, P. Micke, N. Scharnhorst, I. D. Leroux, J. R. Crespo López-Urrutia, and P. O. Schmidt. A tunable low-drift

laser stabilized to an atomic reference. *Applied Physics B*, 122(9):236, Aug 2016. [Cited on pages 13 and 18.]

[27] C. W. Chou, D. B. Hume, J. C. J. Koelemeij, D. J. Wineland, and T. Rosenband. Frequency comparison of two high-accuracy Al$^+$ optical clocks. *Phys. Rev. Lett.*, 104:070802, Feb 2010. [Cited on page 13.]

[28] Nils Scharnhorst, Javier Cerrillo Moreno, Johannes Kramer, Ian D. Leroux, Jannes B. Wübbena, Alex Retzker, and Piet O. Schmidt. Multi-mode double-bright EIT cooling. *arXiv:1711.00738*, 2017. [Cited on pages 13, 15, 30, 33, and 34.]

[29] Nils Scharnhorst, Javier Cerrillo Moreno, Johannes Kramer, Ian D. Leroux, Jannes B. Wübbena, Alex Retzker, and Piet O. Schmidt. Experimental and theoretical comparison of the cooling performance between standard and double-bright EIT cooling. *arXiv:1711.00732*, 2017. [Cited on pages 13, 15, 18, 30, 31, 33, 34, 35, and 36.]

[30] Regina Lechner, Christine Maier, Cornelius Hempel, Petar Jurcevic, Ben P. Lanyon, Thomas Monz, Michael Brownnutt, Rainer Blatt, and Christian F. Roos. Electromagnetically-induced-transparency ground-state cooling of long ion strings. *Physical Review A*, 93(5), May 2016. [Cited on pages 14 and 20.]

[31] S. T Cundiff and J. Ye. Colloquium: Femtosecond optical frequency combs. *Reviews of Modern Physics*, 75(1):325–342, 2003. [Cited on page 16.]

[32] Jörn Stenger, Harald Schnatz, Christian Tamm, and Harald Telle. Ultraprecise Measurement of Optical Frequency Ratios. *Physical Review Letters*, 88(7):073601, February 2002. [Cited on pages 16 and 33.]

[33] Robert Löw, Hendrik Weimer, Johannes Nipper, Jonathan B Balewski, Björn Butscher, Hans Peter Büchler, and Tilman Pfau. An experimental and theoretical guide to strongly interacting Rydberg gases. *Journal of Physics B: Atomic, Molecular and Optical Physics*, 45(11):113001, 2012. [Cited on page 17.]

[34] J. G. Danzl, E. Haller, M. Gustavsson, M. J. Mark, R. Hart, N. Bouloufa, O. Dulieu, H. Ritsch, and H.-C. Nagerl. Quantum Gas of Deeply Bound Ground State Molecules. *Science*, 321(5892):1062–1066, August 2008. [Cited on page 17.]

[35] David R. Leibrandt, Michael J. Thorpe, James C. Bergquist, and Till Rosenband. Field-test of a robust, portable, frequency-stable laser. *Optics Express*, 19(11):10278–10286, May 2011. [Cited on page 17.]

[36] B. Parker, G. Marra, L. A. M. Johnson, H. S. Margolis, S. A. Webster, L. Wright, S. N. Lea, P. Gill, and P. Bayvel. Transportable cavity-stabilized laser system for optical carrier frequency transmission experiments. *Appl. Opt.*, 53(35):8157–8166, Dec 2014. [Cited on page 17.]

[37] Kai Bongs, Yeshpal Singh, Lyndsie Smith, Wei He, Ole Kock, Dariusz Świerad, Joshua Hughes, Stephan Schiller, Soroosh Alighanbari, Stefano Origlia, Stefan Vogt, Uwe Sterr, Christian Lisdat, Rodolphe Le Targat, Jérôme Lodewyck, David Holleville, Bertrand Venon, Sébastien Bize, Geoffrey P. Barwood, Patrick Gill, Ian R. Hill, Yuri B. Ovchinnikov, Nicola Poli, Guglielmo M. Tino, Jürgen Stuhler, and Wilhelm Kaenders. Development of a strontium optical lattice clock for the SOC mission on the ISS. *Comptes Rendus Physique*, 16(5):553 – 564, 2015. The measurement of time / La mesure du temps. [Cited on page 17.]

[38] Mariia Stepanova. Setup of a logic laser for Ca^+. Master's thesis, Leibniz Universität Hannover, 2017. [Cited on page 17.]

[39] B. C. Young, F. C. Cruz, W. M. Itano, and J. C. Bergquist. Visible lasers with subhertz linewidths. *Physical Review Letters*, 82(19):3799–3802, 1999. [Cited on page 18.]

[40] T. Kessler, C. Hagemann, C. Grebing, T. Legero, U. Sterr, F. Riehle, M. J. Martin, L. Chen, and J. Ye. A sub-40-mHz-linewidth laser based on a silicon single-crystal optical cavity. *Nature Photonics*, 6:687–692, 2012. [Cited on page 18.]

[41] Sebastian Häfner, Stephan Falke, Christian Grebing, Stefan Vogt, Thomas Legero, Mikko Merimaa, Christian Lisdat, and Uwe Sterr. $8x10^{-17}$ fractional laser frequency instability with a long room-temperature cavity. *Optics Letters*, 40(9):2112, May 2015. [Cited on page 18.]

[42] H. L. Stover and W. H. Steier. Locking of laser oscillators by light injection. *Applied Physics Letters*, 8(4):91–93, 1966. [Cited on page 18.]

[43] F. Diedrich, J. C. Bergquist, W. M Itano, and D. J. Wineland. Laser cooling to the zero-point energy of motion. *Physical Review Letters*, 62(4):403–406, 1989. [Cited on page 20.]

[44] C. Monroe, D. M. Meekhof, B. E. King, S. R. Jefferts, W. M. Itano, D. J. Wineland, and P. Gould. Resolved-sideband Raman cooling of a bound atom to the 3D zero-point energy. *Physical review letters*, 75(22):4011–4014, 1995. [Cited on page 20.]

[45] Ch. Roos, Th. Zeiger, H. Rohde, H. C. Nägerl, J. Eschner, D. Leibfried, F. Schmidt-Kaler, and R. Blatt. Quantum State Engineering on an Optical Transition and Decoherence in a Paul Trap. *Physical Review Letters*, 83(23):4713–4716, December 1999. [Cited on page 20.]

[46] Vladan Vuletić, Cheng Chin, Andrew J. Kerman, and Steven Chu. Degenerate Raman Sideband Cooling of Trapped Cesium Atoms at Very High Atomic Densities. *Physical Review Letters*, 81(26):5768–5771, 1998. [Cited on page 20.]

[47] D. J Han, S. Wolf, S. Oliver, C. McCormick, M. T DePue, and D. S Weiss. 3D Raman sideband cooling of cesium atoms at high density. *Physical Review Letters*, 85(4):724–727, 2000. [Cited on page 20.]

[48] S. E. Hamann, D. L. Haycock, G. Klose, P. H. Pax, I. H. Deutsch, and P. S. Jessen. Resolved-sideband Raman cooling to the ground state of an optical lattice. *Physical review letters*, 80(19):4149–4152, 1998. [Cited on page 20.]

[49] Giovanna Morigi, J Eschner, and Ch Keitel. Ground state laser cooling using electromagnetically induced transparency. *Phys. Rev. Lett.*, 85(21):4458–61, 2000. [Cited on page 20.]

[50] C. F. Roos, D. Leibfried, A. Mundt, F. Schmidt-Kaler, J. Eschner, and R. Blatt. Experimental demonstration of ground state laser cooling with electromagnetically induced transparency. *Physical Review Letters*, 85(26):5547–5550, 2000. [Cited on page 20.]

[51] Y. Lin, J. P. Gaebler, T. R. Tan, R. Bowler, J. D. Jost, D. Leibfried, and D. J. Wineland. Sympathetic Electromagnetically-Induced-Transparency Laser Cooling of Motional Modes in an Ion Chain. *Physical Review Letters*, 110(15):153002, April 2013. [Cited on page 20.]

[52] Tobias Kampschulte, Wolfgang Alt, Sebastian Manz, Miguel Martinez-Dorantes, René Reimann, Seokchan Yoon, Dieter Meschede, Marc Bienert, and Giovanna Morigi. Electromagnetically-induced-transparency control of single-atom motion in an optical cavity. *Phys. Rev. A*, 89:033404, Mar 2014. [Cited on page 20.]

[53] Jannes B. Wübbena. *Controlling Motion in Quantum Logic Clocks*. PhD Thesis, Leibniz Universität Hannover, July 2014. [Cited on pages 21 and 29.]

[54] Huber Gerhard T. *Quantum thermodynamics with trapped ions*. PhD thesis, Universität Ulm, 2010. [Cited on page 21.]

[55] T. Rosenband, W. M Itano, P. O Schmidt, D. B Hume, J. C. J Koelemeij, J. C Bergquist, and D. J Wineland. Blackbody radiation shift of the $^{27}Al^+$ $^1S_0$ - $^3P_0$ transition. In *Proceedings of the 20th European Frequency and Time Forum*, pages 289–291, Braunschweig, Germany, 2006. [Cited on pages 24, 31, and 32.]

[56] M. S. Safronova, M. G. Kozlov, and Charles W. Clark. Precision Calculation of Blackbody Radiation Shifts for Optical Frequency Metrology. *Physical Review Letters*, 107(14):143006, 2011. [Cited on pages 24 and 25.]

[57] M. Doležal, P. Balling, P. B. R. Nisbet-Jones, S. A. King, J. M. Jones, H. A. Klein, P. Gill, T. Lindvall, A. E. Wallin, M Merimaa, C. Tamm, C. Sanner, N. Huntemann, N. Scharnhorst, I. D. Leroux, P. O. Schmidt, T. Burgermeister, T. E. Mehlstäubler, and E. Peik. Analysis of thermal radiation in ion traps for optical frequency standards. *Metrologia*, 52(6):842, 2015. [Cited on page 24.]

[58] D. J. Berkeland, J. D. Miller, J. C. Bergquist, W. M. Itano, and D. J. Wineland. Minimization of ion micromotion in a Paul trap. *Journal of Applied Physics*, 83(10):5025–5033, 1998. [Cited on pages 25, 26, and 28.]

[59] J. Keller, H. L. Partner, T. Burgermeister, and T. E. Mehlstäubler. Precise determination of micromotion for trapped-ion optical clocks. *Journal of Applied Physics*, 118(10):104501, September 2015. [Cited on page 26.]

[60] A. Kramida, Yu. Ralchenko, J. Reader, and and NIST ASD Team. NIST Atomic Spectra Database (ver. 5.3). NIST Atomic Spectra Database (ver. 5.3), [Online]. Available: http://physics.nist.gov/asd [2017, October 24]. National Institute of Standards and Technology, Gaithersburg, MD., 2015. [Cited on pages 31 and 32.]

[61] M. Hettrich, T. Ruster, H. Kaufmann, C. F. Roos, C. T. Schmiegelow, F. Schmidt-Kaler, and U. G. Poschinger. Measurement of dipole matrix elements with a single trapped ion. *Phys. Rev. Lett.*, 115:143003, Oct 2015. [Cited on page 31.]

[62] J. Evers and C. H. Keitel. Double-EIT ground-state laser cooling without blue-sideband heating. *EPL*, 68(3):370, November 2004. [Cited on pages 33 and 35.]

[63] M Guggemos, D Heinrich, O A Herrera-Sancho, R Blatt, and C F Roos. Sympathetic cooling and detection of a hot trapped ion by a cold one. *New Journal of Physics*, 17(10):103001, 2015. [Cited on page 36.]

List of Figures

Publications

Scientific publications

[1] Y. Wan, F. Gebert, J.B. Wübbena, **N. Scharnhorst**, S. Amairi, I.D. Leroux, B. Hemmerling, N. Lörch, K. Hammerer, P.O. Schmidt, *Precision spectroscopy by photon-recoil signal amplification*, Nature Communications **5**, 4096 (2014)

[2] **N. Scharnhorst**, J.B. Wübbena, S. Hannig, K. Jakobsen, J. Kramer, I.D. Leroux, and P.O. Schmidt, *High-bandwidth transfer of phase stability through a fiber frequency comb*, Optics Express **23**, Issue 15, 19771-19776 (2015)

[3] M. Doležal, P. Balling, P.B.R. Nisbet-Jones, S.A. King, J.M. Jones, H.A. Klein, P. Gill, T. Lindvall, A.E. Wallin, M. Merimaa, C. Tamm, C. Sanner, N. Huntemann, **N. Scharnhorst**, I.D. Leroux, P.O. Schmidt, T. Burgermeister, T.E. Mehlstäubler, E. Peik, *Analysis of thermal radiation in ion traps for optical frequency standards*, Metrologia **52**, 842-56 (2015)

[4] T. Leopold, L. Schmöger, S. Feuchtenbeiner, C. Grebing, P. Micke, **N. Scharnhorst**, I. D. Leroux, J. R. Crespo Lòpez-Urrutia, P. O. Schmidt, *A tunable low-drift laser stabilized to an atomic reference*, Appl. Phys. B (2016) 122: 236

[5] I.D. Leroux, **N. Scharnhorst**, S. Hannig, J. Kramer, L. Pelzer, M. Stepanova, P.O. Schmidt, *On-line estimation of local oscillator noise and optimisation of servo parameters in atomic clocks*, Metrologia **54**, 307-321 (2017)

[6] **N. Scharnhorst**, J. Cerrillo Moreno, J. Kramer, I.D. Leroux, J.B. Wübbena, P.O. Schmidt, *Multi-mode double-bright EIT cooling*, arXiv:1711.00738 (2017)

[7] **N. Scharnhorst**, J. Cerrillo Moreno, J. Kramer, I.D. Leroux, J.B. Wübbena, P.O. Schmidt, *Experimental and theoretical comparison of the cooling performance between standard and double-bright EIT cooling*, arXiv:1711.00732 (2017)

Talks

[1] JRP Satellite Workshop on SIB04, Neuchâtel, Schweiz, *The Al$^+$ clock at PTB*
     (2014/06)

[2] DPG Frühjahrstagung, Heidelberg, *Suppressing high-frequency noise in phase-locks
     to fiber frequency combs* (2015/03)

Posters

[1] IonTech, Siegen:*Towards a portable Al$^+$ clock using quantum logic* (2012/05)

[2] DPG Frühjahrstagung, Hannover, *Laser stabilization to a frequency comb for an
     optical clock* (2013/03)

[3] International School of Physics "Enrico Fermi", Course 189 "Ion Traps for Tomor-
     rows Application", Varenna, Italien: *Laser stabilization to a frequency comb for
     an optical clock* (2013/07)

Curriculum Vitae

Personal Data

Name
    Nils Scharnhorst
born on 6th of December 1986 in Hannover
unmarried, german

Doctorate

07/2017–today   **Leibniz Universität Hannover**, Research assistant

01/2012–06/2017   **Physikalisch-Technische Bundesanstalt**, Research assistant

University education

October 2011   **Leibniz Universität Hannover**, Degree: Master of Science, thesis title: *Untersuchung von Auswahlregeln und Spindynamik in* $^{28}Si{:}P$

2009–2011   **Leibniz Universität Hannover**, Master student of physics

October 2009   **Leibniz Universität Hannover**, Degree: Bachelor of Science, thesis title: *Charakterisierung eines Ultrakurzpuls-Hochleistungslasers*

2006–2009   **Leibniz Universität Hannover**, Bachelor student of physics

Alternative service

2005–2006   Technical service **Altenpflegeheim Marienhaus**, Gellertstraße 51, 30175 Hannover

Formal education

2005   Abitur, **Gymnasium St.-Ursula-Schule** in Hannover

Acknowledgments

I would like to thank Piet O. Schmidt for giving me the opportunity to write this PhD thesis at the QUEST Institute of Experimental Quantum Metrology at the Physikalisch-Technische Bundesanstalt and the Leibniz Universität Hannover, and for his professional advice.

I thank the current and former members of the group for the good working spirit and friendly atmosphere. Special thanks go to Jannes B. Wübbena. As my predeccessor he introduced me to the experiment and patiently answered all the many questions I had! Javier Cerillo Moreno from the TU Berlin deserves thanks for his theoretical support and the many helpful discussions about all EIT related stuff. My thanks also go to Ian D. Leroux who joined the experiment as post-doc and who helped a lot with his efficient approaches and his almost encyclopaedic physics knowledge, I also owe him a great improvement in my English skills. As my successor on the iqloc experiment I want to thank Johannes Kramer for his help in the lab. I would like to thank Florian Gebert. Together we had many stimulating and productive discussions. I would like to thank Stephan Hannig as part-time fellow PhD student at the iqloc I experiment, especially during time of 'the incident'. Thanks also go to Birgit Ohlendorf for her help concerning all organisational stuff related to PhD students, doctorate.

There are very many people who also deserve thanks: From the iqloc experiment: Lennart Pelzer, Nicolas Spethmann Olaf Mandel. From the Difcos experiment: Yong, Fabian, Jan Christoph, and Chunyan. From the HiChI experiment: Tobias L., and Steven. From the MIT experiment: Tanja, Jonas, Tobias, Karsten and Jan. From the electronic workshop: Julia, and Peter. From the mechanics workshop: Sven, Alex, and Rebecca.

I would like to thank all those people not only for their nice work atmosphere but also the nice time that were spent during leisure time!

Further thanks go to Gesine Grosche, Thomas Legero, Erik Benkler and Sebastian Raupach for their help with the fibre length stabilisation and our master laser, as well as to Burghard Lipphardt for his value input on locking electronics and frequency combs.

Last, but definitively not least, I want to thank my parents and my sister for their support and help. Without them I would have not gotten to where I am now, and I hope they know how much I value having them!